Cerium Dioxide Nanoparticles Induce Apoptosis and Autophagy in Human Peripheral Blood Monocytes

Salik Hussain,[†,*] Faris Al-Nsour,[†] Annette B. Rice,[†] Jamie Marshburn,[†] Brenda Yingling,[†] Zhaoxia Ji,[‡] Jeffrey I. Zink,[‡] Nigel J. Walker,[§] and Stavros Garantziotis[†]

[†]Clinical Research Unit, National Institute of Environmental Health Sciences (NIEHS)/National Institute of Health (NIH), Research Triangle Park 27709, North Carolina, United States, [‡]UC Center for Environmental Implications of Nanotechnology, University of California, Los Angeles, California, United States, and [§]Division of the National Toxicology Program (NTP), National Institute of Environmental Health Sciences (NIEHS)/National Institute of Health (NIH), Research Triangle Park 27709, North Carolina, United States

ABSTRACT

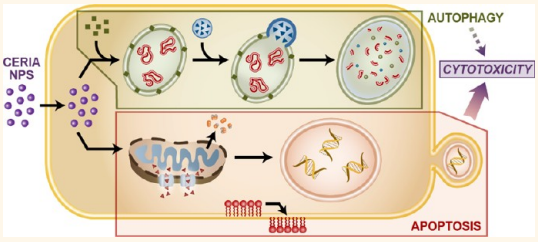

Cerium dioxide nanoparticles (CeO_2 NPs) have diversified industrial uses, and novel therapeutic applications are actively being pursued. There is a lack of mechanistic data concerning the effects of CeO_2 NPs on primary human cells. We aimed at characterizing the cytotoxic effects of CeO_2 NPs in human peripheral blood monocytes. CeO_2 NPs and their suspensions were thoroughly characterized, including using transmission electron microscopy (TEM), dynamic light scattering, and zeta potential analysis. Blood from healthy human volunteers was drawn through phlebotomy, and CD14+ cells were isolated. Cells were exposed to CeO_2 NPs (0.5−10 μg/mL) for 20 or 40 h, and mechanisms of cell injury were studied. TEM revealed that CeO_2 NPs are internalized by monocytes and are found either in vesicles or free in the cytoplasm. CeO_2 NP exposure leads to decrease in cell viability, and treated cells exhibit characteristic hallmarks of apoptosis (activation of Bax, loss of mitochondrial membrane potential, DNA fragmentation). CeO_2 NP toxicity is caused by mitochondrial damage and overexpression of apoptosis inducing factor, but is not due to caspase activation or reactive oxygen species production. Moreover, CeO_2 NP exposure leads to autophagy, which is further increased after pharmacological inhibition of tumor suppressor protein p53. Inhibition of autophagy partially reverses cell death by CeO_2 NPs. It is concluded that CeO_2 NPs are toxic to primary human monocytes at relatively low doses.

KEYWORDS: cerium dioxide/ceria · nanoparticle · toxicity · apoptosis · autophagy · monocytes · ultrafine

Nanoparticle-size cerium dioxide (CeO_2 NPs) has gained increased attention in the recent past, due to its diverse uses. In industrial settings CeO_2 NPs are used in catalysis, ultraviolet absorbance, oxygen sensing, solar and fuel cells, and polishing (for glasses, lenses, television tubes, fuel cells, and precision optics).[1−5] In addition to these industrial applications, CeO_2 NP use in therapeutics has also been proposed, such as in antioxidant therapy, neuroprotection, radioprotection, and ocular protection.[6−10] Furthermore, CeO_2 NPs are of significant environmental health interest, since diesel fuel additives containing CeO_2 NPs are used in many countries to reduce the emission of particulate matter from diesel engines.[11] However, the human health effects of the resultant increased emission of CeO_2 NPs are unknown. According to the Health Effects Institute (HEI) CeO_2 NP emissions were expected to reach up to 22 million pounds annually in the European Union after introduction of diesel-additive nano CeO_2.[12] Importantly, most of the CeO_2 released as a result of combustion is in the form of NPs.[13] For all these reasons, the Organization for Economic Cooperation and Development (OECD) has included CeO_2 NPs in the priority list of the nanomaterials requiring urgent evaluation.[14]

Health effects of NPs in general and CeO_2 NPs in particular are still a matter of continued debate. *In vitro* and *in vivo* experiments suggest that CeO_2 NPs produce reactive oxygen species (ROS), inflammation, lipid peroxidation, lung damage, and altered macrophage phenotypes.[15,16] Furthermore, CeO_2 NPs have acute and chronic fibrotic and inflammatory effects in murine lungs.[17] However, there are also reports of CeO_2 NPs acting as antioxidant and anti-inflammatory agents.[18,19] Variability in examined target species and cell type, experimental setup (exposure concentration and duration), and NPs used (shape, size, purity, and surface modifications) complicates the accurate assessment of CeO_2 NPs' effects.

* Address correspondence to salik.hussain@nih.gov.

Received for review December 28, 2011 and accepted June 20, 2012.

Published online June 21, 2012
10.1021/nn302235u

TABLE 1. Characteristics of CeO_2 NPs

primary size		hydrodynamic diameter						zeta potential mV			
TEM/ SEM, nm	XRD, nm	*ex vivo*, nm	water, nm	phase and structure (XRD)	surface area (BET), $m^2\ g^{-1}$	pH_{iep}[a]	morphology (TEM)	*ex vivo* (pH 7.0), mV	water (pH 6.1), mV	pDi[b]	EPM,[c] $m^2\ V^{-1}\ s^{-1}$
10−30	7	194(30)	231(16)	100% cubic ceria	93.8	7.8	irregular	−15(3)	19.1(6)	0.45	$(1.49 \pm 0.48) \times 10^{-8}$

[a] Isoelectric point. [b] Polydispersity index. [c] Electrophoretic mobility (in water).

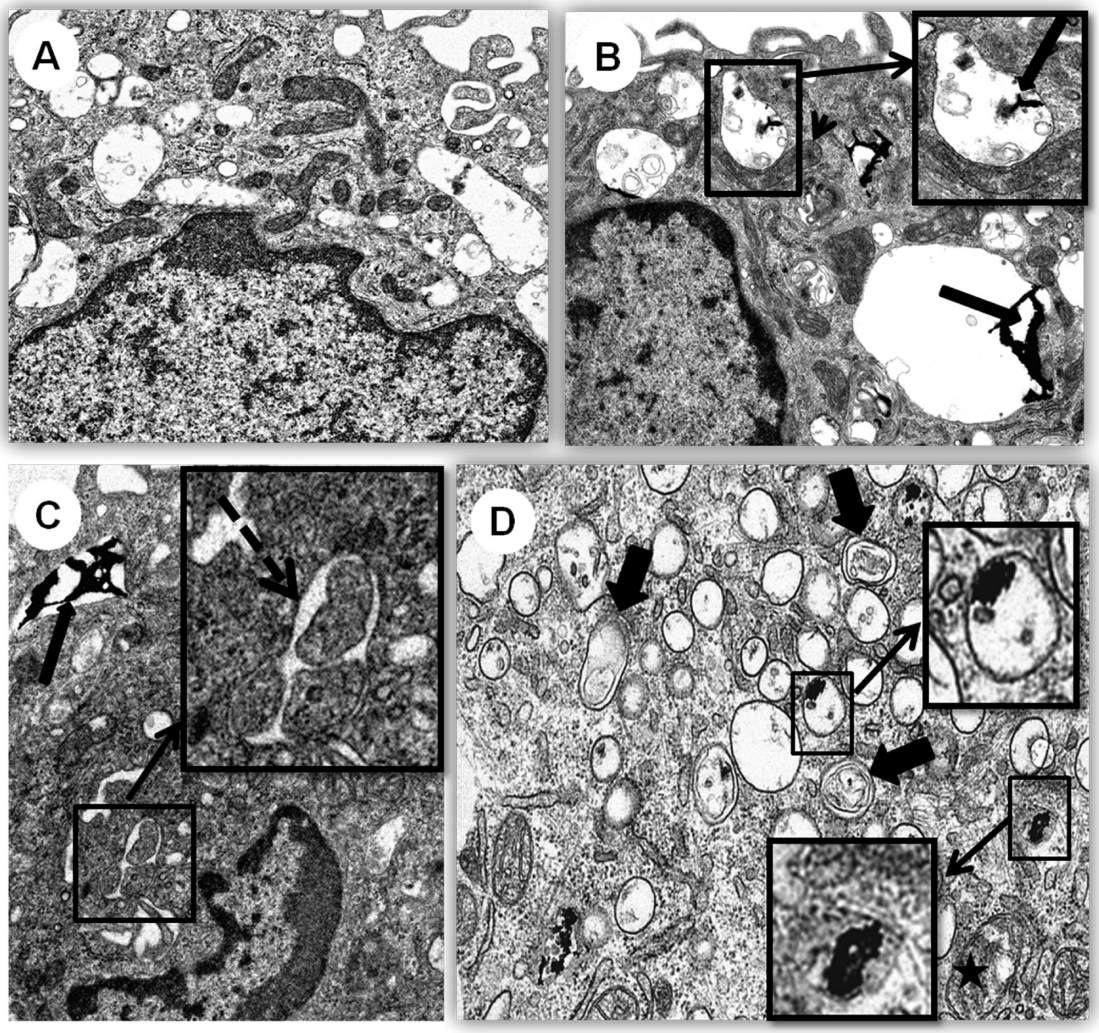

Figure 1. TEM analysis of human monocytes after CeO_2 NP exposure. Cells were treated with 10 μg/mL CeO_2 NPs for 40 h before analysis. Photo micrographs of (A) control and (B, C, and D) CeO_2 NP-treated cells. Intracellular accumulation of CeO_2 NPs in vesicles (long arrows), enlargement of mitochondria (arrowhead), autophagic vesicle formation (broken arrow), autolysosomes (thick short arrows), swollen mitochondria (asterisk). Insets present detailed structure of vesicle containing an aggregate of CeO_2 NPs (B), autophagic vesicle (C), and ceria NPs inside vesicles and free in cytoplasm (D). (A, B, and C) 9900×, (D) 20 500×.

It is now known that different modalities of cell death (apoptosis, necrosis, autophagy) contribute to the pathophysiology of different human disorders (cancer, neurodegenerative diseases, sepsis, *etc.*).[20−22] Moreover, it has been shown that autophagy (generally thought to be a survival mechanism) is also a programmed cell death process besides apoptosis.[23] A better understanding of the interaction of NPs with these pathways of cell injury can help in developing the counter strategies for different human disorders and will help in the formulation of safe and consumer-friendly nanotechnology. Keeping in view the proposed nanomedical applications of CeO_2 NPs, an evaluation of such interactions becomes even more pertinent, as these could result in potential unwanted consequences.

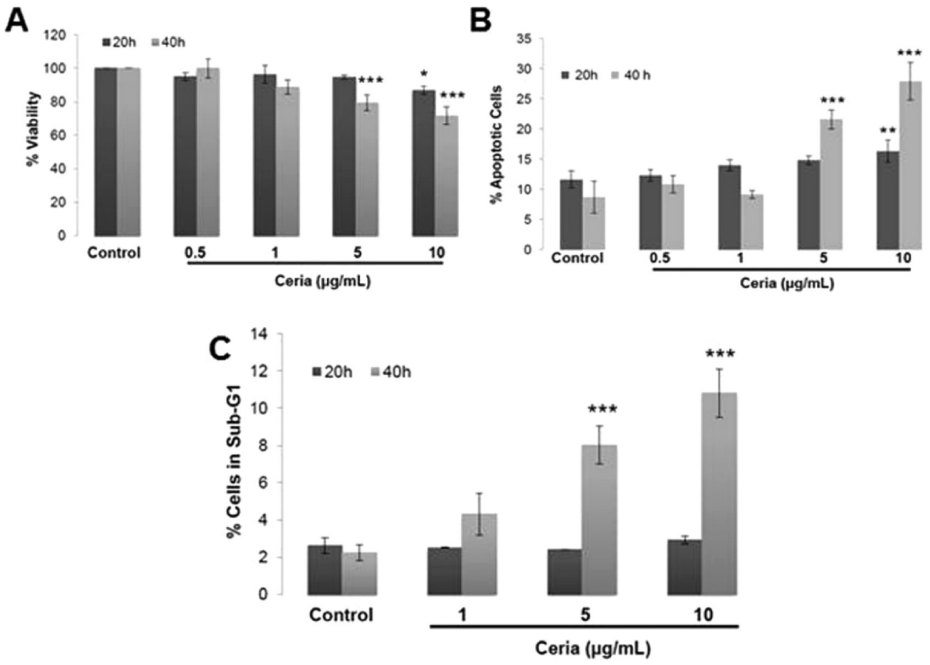

Figure 2. Cell death detection after CeO_2 NP exposure. Cells were treated with different doses (0.5−10 μg/mL) of CeO_2 NPs for either 20 or 40 h and analyzed for (A) cell viability by calcein-AM staining and analyzed by spectrofluorimetry. (B) Cell death (apoptosis *vs* necrosis) detection by staining with annexin/PI and analyzed by flow cytometery. Results are presented as % apoptotic cells (early + late apoptotic cells). More than 90% of the cells were annexin positive and PI negative (A+/PI−). (C) DNA fragmentation by measuring the sub-G1 peak through flow cytometery. Data were analyzed by analysis of variance (ANOVA) followed by the Bonferroni *post hoc* test. Graphs show average ± SD, $n = 3-5$. *$p < 0.05$, **$p < 0.01$, and ***$p < 0.001$.

Most studies addressing potential toxic effects of CeO_2 NPs were performed in either immortalized cell lines or nonhuman cells. Furthermore, doses used in some of the studies far exceed what is likely to be a relevant range for human environmental or pharmacological exposure. We therefore studied effects of low-dose (nM−μM) CeO_2 NPs in cultures of human primary monocytes. We demonstrate that CeO_2 NP exposure leads to the cytotoxicity in monocytes associated with an induction of mitochondria-mediated apoptosis and autophagy. To the best of our knowledge, this is the first report on the effects of CeO_2 NPs in primary human cells in general and in human peripheral blood monocytes in particular.

RESULTS

NP Characterization. Detailed physicochemical characteristics of CeO_2 NPs in the dry state and after suspending in cell culture medium or water are presented in Table 1 and Supplementary Figure S1. In the environment CeO_2 will exist likely as both dispersed and aggregated forms. Respirable "particle" size is <3 μm, so NP sizes and aggregates are relevant for human exposures. TEM images of NPs are shown in Supplementary Figure S2, showing the irregular shape and aggregation of CeO_2 NPs.

CeO_2 NPs Induce Ultrastructural Alterations. TEM analysis revealed that CeO_2 NPs are incorporated by CD14+ cells (Figure 1). CeO_2 NPs were found inside cells as electron dense material either free in the cytoplasm or as membrane-bound aggregates. Pathological changes included an increase in phagolysosomes, an increase in Golgi (with minimal dilated cisterns), increased formation of autophagic vesicles, and a mild increase in mitochondrial swelling together with mitochondrial elongation. Phagolysosomes had CeO_2 NPs, cellular debris, myelin figures, membrane fragments, and occasionally small lipid droplets. Most cells showed diffuse cytoplasmic expansion after exposure to CeO_2 NPs.

CeO_2 NPs Induce Apoptosis. After 40 h exposure to 5 and 10 μg/mL CeO_2 NPs a significant decrease in viability of monocytes was observed (Figure 2 A). Further evaluation of the mode of cell death revealed that this loss of viability was mainly due to apoptosis (Figure 2B). Moreover, we observed significant DNA fragmentation after exposure to CeO_2 NPs (Figure 2C).

CeO_2 NPs Induce Mitochondrial Damage. A significant number of cells (20−25%) with the activated form of a pro-apoptotic protein, Bax (relocated to the mitochondria), were observed following 5 and 10 μg/mL CeO_2 NP exposure for 40 h (Figure 3A, B). An increase in mitochondrial depolarization (loss of mitochondrial membrane potential; $\downarrow\Delta\Psi_m$) was also observed after CeO_2 NP exposures (Figure 3C). It is noteworthy that we did not observe activation of caspase 3/7 after exposure to CeO_2 NPs, and pretreatment with pan-caspase inhibitor (Z-Vad Fmk) did not protect from apoptosis (Supplementary Figure S3). However, an increase in the protein levels of apoptosis inducing factor (AIF), known to induce caspase-independent apoptosis and DNA fragmentation, was observed after NP

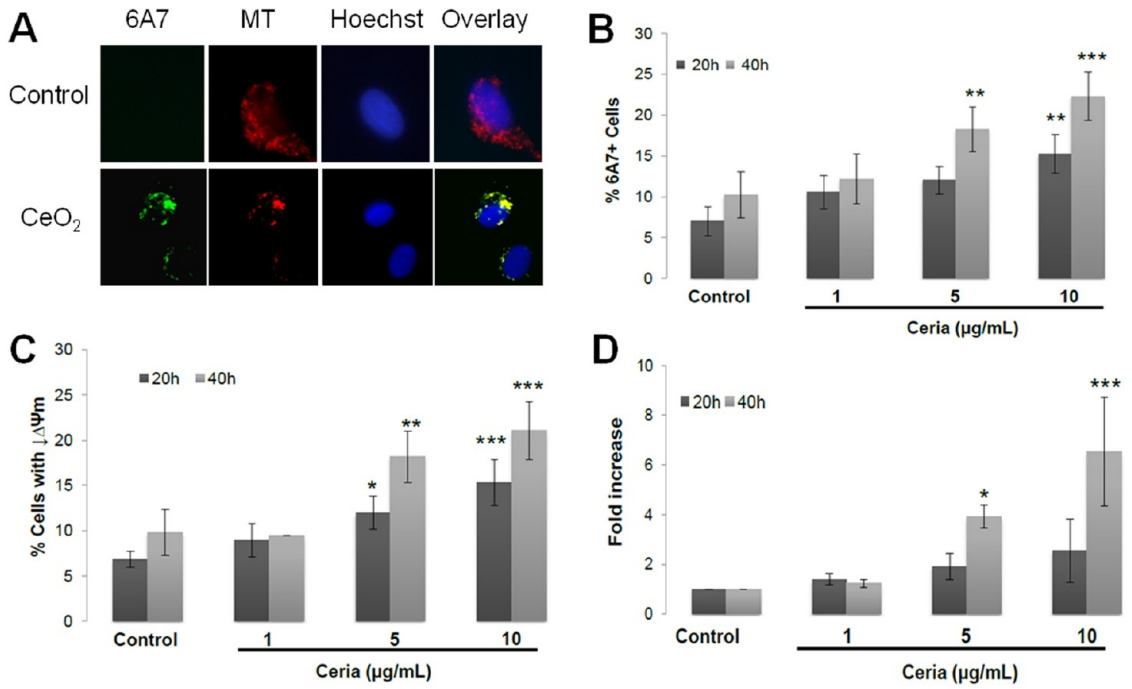

Figure 3. Mitochondrial alterations after CeO_2 NP exposure. Cells were treated with different doses (1−10 μg/mL) of CeO_2 NPs for either 20 or 40 h and analyzed for (A) activation and mitochondrial relocation of pro-apoptotic protein Bax. Immunofluorescent images of cells showing activated form of Bax relocating to mitochondria (co-localized with MitoTracker Red (MT)-labeled mitochondria). (B) Percent of 6A7 positive cells. At least 600 stained cells from each individual were counted to determine the percent of 6A7 positive cells. (C) Loss of mitochondrial membrane potential ($\Delta\Psi_m$) after staining with JC-1 probe. Cells were analyzed through flow cytometery. (D) AIF protein expression. Cells were stained with specific antibody for AIF and analyzed through flow cytometery. Results are presented as fold increase with respect to control (calculated using mean fluorescence intensity of the populations). Data were analyzed by analysis of variance (ANOVA) followed by the Bonferroni *post hoc* test. Graphs show average ± SD, $n = 3-5$. *$p < 0.05$, **$p < 0.01$, and ***$p < 0.001$.

exposures (Figure 3D). A mild ROS production response was noted after exposure to CeO_2 NPs (Supplementary Figure S4). This ROS appeared to be mainly composed of superoxide anions ($O_2^{\bullet -}$) produced due to mitochondrial damage (Supplementary Figure S5). However, successful inhibition of $O_2^{\bullet -}$ production using PEG-catalase failed to prevent cells from undergoing apoptosis (Supplementary Figure S5).

CeO_2 NPs Induce Autophagy. CeO_2 NP exposure led to a significant increase in LysoTracker Red uptake (Figure 4A) and increased the number of LC3b+ vesicles (Figure 4B, C). These results were further confirmed by detection of monodansylcadaverine (MDC) positive autophagic vacuoles (data not shown).

p53 Inhibition Amplifies CeO_2 NP-Induced Autophagy. As p53 can differentially regulate both apoptosis and autophagy, we further explored whether p53 inhibition (using the pharmacological inhibitor pifithrin-α (PFT-α)) can modulate CeO_2 NP-induced apoptosis and autophagy (Figure 5). We observed that p53 inhibition has no effect on CeO_2 NP-induced apoptosis (Figure 5A, B); however it leads to an increase in autophagy (Figure 5C).

Crosstalk between CeO_2 NP-Induced Autophagy and Apoptosis. Wortmannin (an autophagy inhibitor) treatment completely inhibited the autophagy induced by CeO_2 NPs (Figure 6A) and led to a 30−58% increase in the viability of CeO_2 NP-treated cells (Figure 6B). This increase in viability was partly (20−35%) due to a decrease in the apoptosis induced by CeO_2 NPs (Figure 6C). These results suggest that autophagy contributes to the cell injury response induced by CeO_2 NPs.

DISCUSSION

This experimentation aimed at deciphering the effects of CeO_2 NPs on human monocytes. We demonstrate a significant toxic response after 20−40 h exposure to CeO_2 NPs, which involved the induction of type 1 and type 2 programmed cell death processes (apoptosis and autophagy). CeO_2 NP-induced apoptosis involved mitochondrial damage and AIF expression. In addition, CeO_2 NP-induced autophagy contributed to the cytotoxicity and was found to be modulated by p53.

We demonstrate here that CeO_2 NP exposure leads to induction of autophagy in a time- and dose-dependent manner in human monocytes. Indeed, exposure to different types of NPs (*e.g.*, fullerenes, quantum dots, rare earth metals) has been shown to induce autophagic events in cultured cells.[24−26] The exact mechanism of CeO_2 NP-induced autophagy is unclear and could involve the direct interaction with endosomes/lysosomes themselves (since CeO_2 NPs appear to accumulate in these compartments), overexpression of genes for vesicle formation, or identification of NPs as foreign endosomal pathogens. Moreover, an association

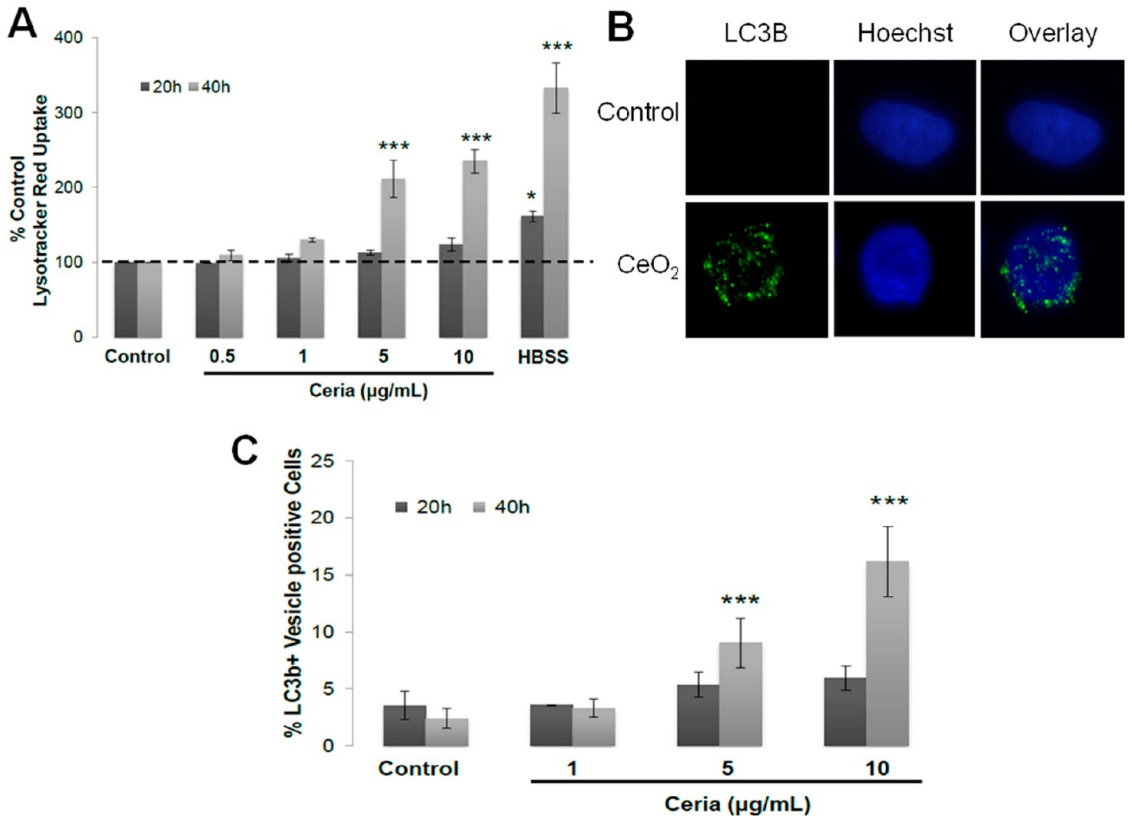

Figure 4. Autophagy detection in CeO_2 NP-treated cells. Cells were treated with increasing doses (1−10 μg/mL) of CeO_2 NPs for 20 or 40 h and analyzed for (A) LysoTracker Red uptake assay. Cells were incubated with 50 nM LysoTracker Red and 10 μM CellTracker Green, and analysis was performed through spectrofluorimetry. Results are presented as % LysoTracker Red uptake with respect to control. Hanks Balanced Salt Solution (HBSS)-treated cells were used as positive control for autophagy. (B) Immunofluorescent images of cells showing LC3b protein marked vesicles. (C) Percent of LC3b+ vesicle-containing cells. At least 600 stained cells from each individual were counted to determine the LC3b positive cells. Data were analyzed by analysis of variance (ANOVA) followed by the Bonferroni *post hoc* test. Graphs show average ± SD, $n = 3-5$. *$p < 0.05$, **$p < 0.01$, and ***$p < 0.001$.

of p53 with either apoptosis or autophagy or even both processes has been recently demonstrated.[27] We therefore explored the role of p53 in CeO_2 NP-induced cell death pathways. Interestingly we found that apoptosis induction after CeO_2 NP exposure is independent of p53 involvement. However a significant increase in autophagy after p53 inhibition was observed. Indeed, Tasdemir *et al.* have recently shown the negative regulation of autophagy by cytoplasmic p53.[28] They demonstrated that depletion or pharmacologic inhibition of cytoplasmic p53 in cell lines and in mice induces autophagy. We show for the first time that in the case of existing autophagic events such p53 inhibition can lead to an increase in autophagy. This could be due to the direct interaction of CeO_2 NPs with cytoplasmic p53. It has been postulated that many of the observed adverse effects of NPs are due to their interaction with proteins, leading to a change in protein conformation and irreversible loss of activity (in the case of enzymes).[29,30] Further experimentation is needed to understand this process in the case of CeO_2 NPs.

The fact that induction of autophagy was mainly observed at the doses causing cytotoxicity suggests that upregulation of autophagy is part of the cytotoxic response. It is now known that autophagy can promote cell death by selectively removing survival factors and prolonged removal of cellular constituents resulting in the demise of cells.[31] In our study the role of autophagy as a contributor to cell death is further confirmed by the fact that pretreatment with the autophagy inhibitor wortmannin causes up to 50% reduction in cell death.

An interesting ultrastructural finding was the swelling and elongation of mitochondria in CeO_2 NP-treated cells. Recently, it has been shown that mitochondrial elongation can also occur due to unopposed mitochondrial fusion during the autophagy process and is an attempt to maintain cell viability.[32] These elongated mitochondria can avoid trapping in the autophagic vesicles due to steric hindrance. It is also known that mitochondrial structural and functional changes play an important role in a wide variety of cellular processes, including apoptosis.[33] We demonstrate mitochondrial damage in human monocytes after CeO_2 NP exposure, leading to the induction of apoptosis. We observed activation and relocation of Bax to the mitochondria and decrease in mitochondrial

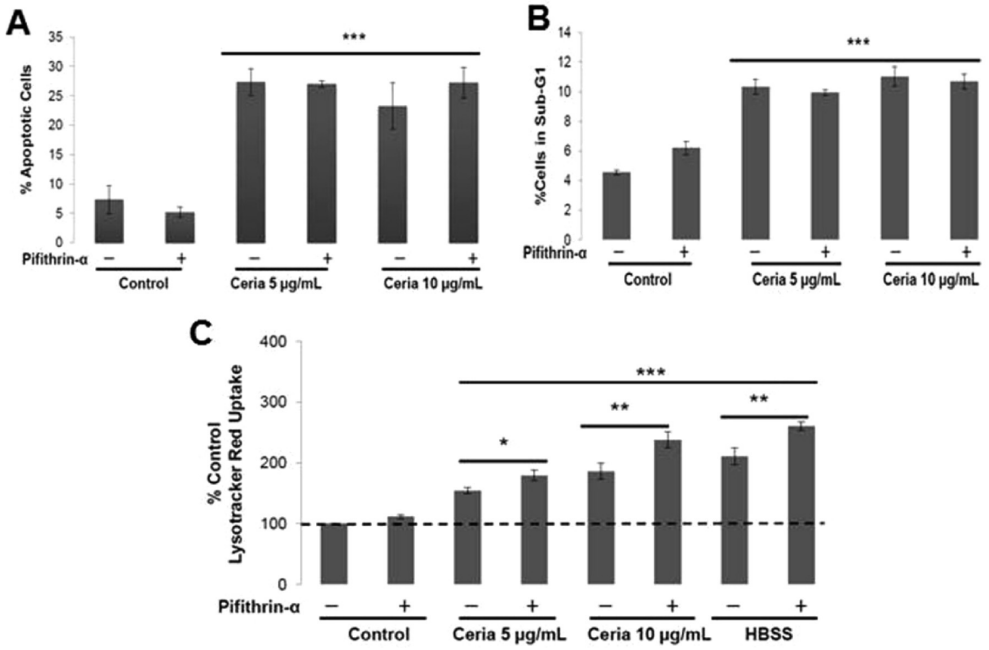

Figure 5. Role of p53 in CeO_2 NP-induced cell death. Cells were preincubated with pifithrin-α for 2 h, treated with CeO_2 NPs (5 or 10 μg/mL) for 20 or 40 h in its presence, and analyzed through flow cytometery for (A) apoptosis detection by annexin-V/PI staining, (B) apoptosis detection through sub-G1 peak estimation, and (C) LysoTracker Red uptake assay. Data were analyzed by analysis of variance (ANOVA) followed by the Bonferroni *post hoc* test. Graphs show average ± SD, $n = 3-5$. *$p < 0.05$, **$p < 0.01$, and ***$p < 0.001$.

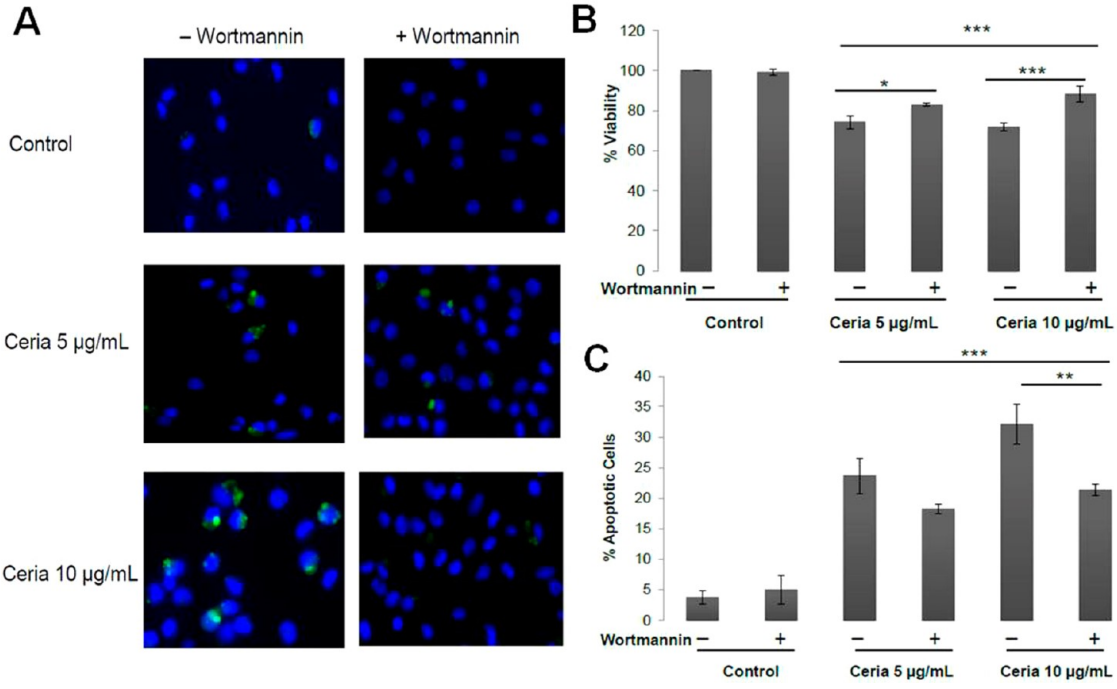

Figure 6. Crosstalk between the autophagy and apoptosis induced by CeO_2 NPs. Cells were preincubated with autophagy inhibitor wortmannin (50 nM) for 2 h and then treated with CeO_2 NPs (5 or 10 μg/mL) for 20 or 40 h in its presence and analyzed for (A) autophagic vesicle formations by MDC staining (nuclei were counterstained with Hoechst), (B) cell viability by calcein-AM staining, and (C) apoptosis detection by annexin-V/PI staining. Data were analyzed by analysis of variance (ANOVA) followed by the Bonferroni *post hoc* test. Graphs show average ± SD, $n = 3-5$ with triplicate of each condition each time. *$p < 0.05$, **$p < 0.01$, and ***$p < 0.001$.

membrane potential ($\downarrow\Delta\Psi_m$) after exposure to CeO_2 NP. This $\downarrow\Delta\Psi_m$ is an early event for the apoptosis process, as it was observed at early time points, while no cell death was evident. Furthermore, apoptosis appeared to be caspase-independent (no activation of caspase 3 or 7 and no protection by a pan-caspase

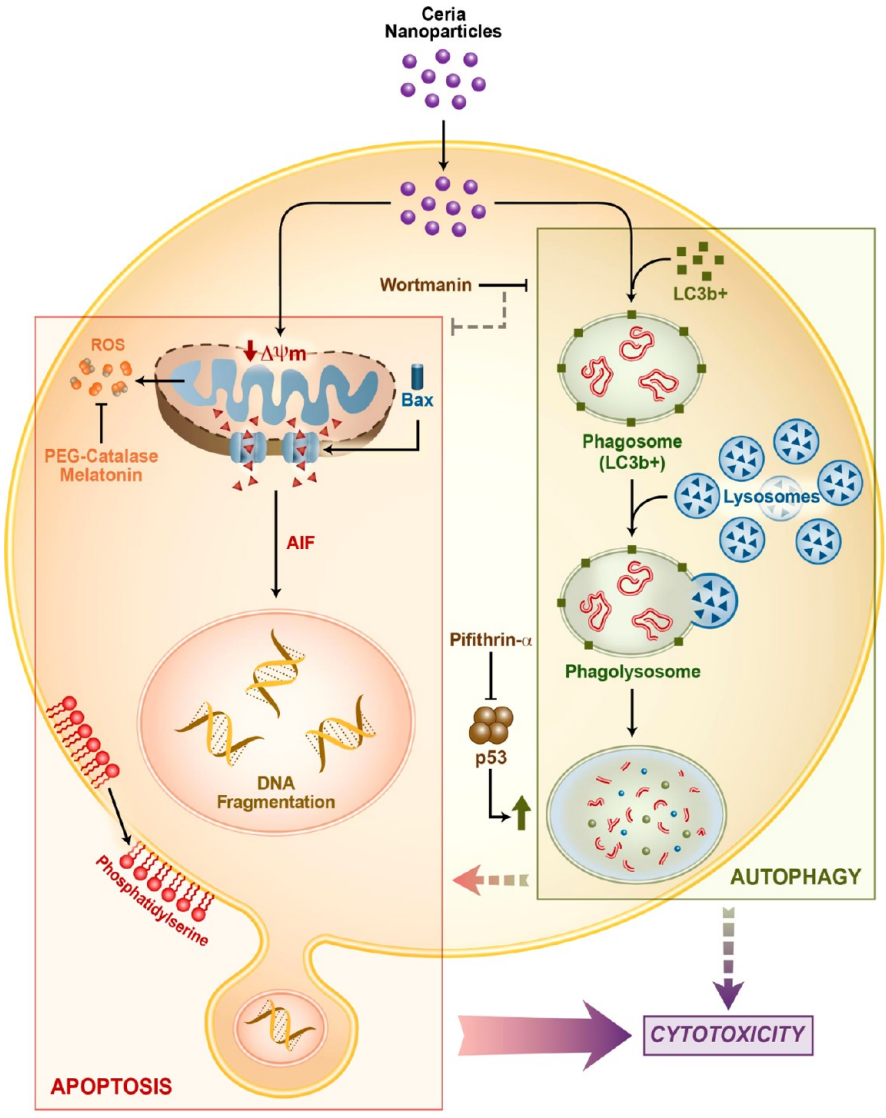

Figure 7. Overview of the CeO_2 NP-induced cell death pathways. CeO_2 NPs induce apoptosis through a mitochondrial pathway (involving activation and mitochondrial localization of Bax, $\downarrow\Delta\Psi_m$, and overexpression of AIF). CeO_2 NP-induced autophagy increased production of LC3b+ phagolysosomes. Inhibition of p53 by pifithrin-α increases the autophagy. Inhibition of autophagy through wortmannin decreases the cytotoxicity, indicating a pro-death role of autophagy.

inhibitor (Zvad-FMK) (Supplementary Figures S3). However, we observed increased protein expression of AIF, which has already been shown to induce caspase-independent apoptosis and DNA fragmentation.[34] Moreover, we show that $O_2^{\bullet -}$ production occurs as a result of mitochondrial damage and does not contribute to cell death induction, since their inhibition does not protect from CeO_2 NP-induced cytotoxicity (Supplementary Figures S4 and S5).

A summary of the mechanisms that we have demonstrated to be involved in CeO_2 NP-induced toxicity is presented in Figure 7. The toxic response to CeO_2 NP exposure is mediated by both autophagy and mitochondrial-mediated apoptosis. Autophagy contributes to cytotoxicity both directly and indirectly, *via* induction of apoptosis. However, mitochondrial damage appears to be the primary mechanism, as autophagy inhibition leads only to approximately 35% reduction in apoptosis induction. These responses seem to be specific to CeO_2 NPs since they did not occur after carbon black NP exposure at similar concentrations and durations (Supplementary Figure S6) and were not a consequence of adsorption of nutrients on the surface of the particles (Supplementary Figure S7).

Our results have significant implications. Human monocytes are an integral part of immunity. Monocytes can initiate or amplify an inflammatory response and are precursors of dendritic cells and tissue macrophages. Moreover, they link innate immunity to adaptive immune responses. Thus monocyte apoptosis by NPs can lead to a lowered ability to mount an effective immune response early after infection, as has been demonstrated for other engineered NPs, particulate matter, and other pollutants.[35−37] Furthermore, recently

it has been shown that autophagy in antigen-presenting cells can lead to the initiation and/or progression of autoimmune processes.[38] Further *in vivo* studies are currently underway in our laboratory to establish the biological relevance of CeO_2 NP-induced monocyte apoptosis *in vivo*.

CONCLUSION

In summary this study provides potential mechanistic pathways for CeO_2 NP-induced cell injury. We demonstrate that CeO_2 NPs induce cytotoxicity through autophagy and a mitochondrial apoptosis pathway in *ex vivo* cultured human peripheral blood monocytes. Further *in vivo* studies are warranted to elaborate the consequences of CeO_2 NPs-induced autophagy and apoptosis. Our results however underscore the urgent need for the rational toxicological assessment of novel nanomaterials at relevant exposure levels. Moreover, for realistic hazard identification of nanomaterials the preferred *in vitro* system should include primary human cells.

METHODS

Nanoparticles. CeO_2 NPs were acquired from Meliorum Technologies (Rochester, NY, USA) and characterized by University of California, Center for Environmental Implications of Nanotechnology (CEIN). NPs were characterized for shape/diameter (transmission electron microscopy (TEM), crystal structure (X-ray diffraction analysis, XRD), surface area (Brunauer–Emmitt–Teller method, BET), suspension behaviors such as hydrodynamic diameter and size distribution (dynamic light scattering), zeta potential (Malvern Zetasizer), purity (thermogravimetric analysis, TGA), and bacterial endotoxins (limulus amebocyte lysate assay). TGA analysis revealed that CeO_2 NPs were 95.14% (wt %) pure and contained 4.1% moisture and 0.85% acid contents. A NP stock solution (1 mg/mL) was prepared in water and stored at 4 °C in a refrigerator. All exposure suspensions were freshly prepared from this stock solution after sonication (3 pulses of 20 s at 235 W each with a 5 s pause) using a Mesonix S 4000 cuphorn sonicator (Qsonica LLC, Newtown, CT, USA). After sonication the particles were suspended in cell culture medium and used to expose cells within 5 min after vortexing.

Dynamic light scattering analysis of CeO_2 NPs suspensions (at the highest utilized concentration; 10 μg/mL) in cell culture medium was done to analyze size distribution and measure zeta potentials of NPs using the ZetaSizer Nano (Malvern Instruments, Westborough, MA, USA). Electrophoretic mobility (an approximation of particle surface charge) was converted into zeta potential using the Helmholtz–Smoluchowski equation.

Study Subjects and Isolation of Cells. This study was approved by the NIEHS Institutional Review Board. Adult human volunteers without history of chronic medical conditions or chronic medication use were recruited to the NIEHS Clinical Research Unit. Population demographics are presented in Supplementary Table S1. Whole blood was withdrawn from an antecubital vein into citrated tubes. Mononuclear fraction was isolated by gradient centrifugation using Histopaque (Sigma Aldrich, St. Louis, MO, USA). Cells were labeled with CD14 magnetic beads and positively selected using a magnetic column according to manufacturer recommendations (Miltenyi Biotec, Boston, MA, USA). By this method 95–99% viable pure human monocytes were obtained, confirmed by flow cytometery and cytospin preparations.

Cells and Culture Conditions. After isolation, cells were seeded in 24-well cell culture plates (400 000 cells per well) in *ex vivo* cell culture medium (Lonza) supplemented with 1% human serum and antibiotics [1% solution of penicillin (100 μg/mL) and streptomycin (100 μg/mL), Invitrogen Carlsbad, CA, USA] and incubated at 37 °C, 5% CO_2, and 95% relative humidity for 2 h. Cell culture medium was then aspirated, and cells were washed thoroughly with fresh medium to remove unattached cells. Cells were then incubated in fresh prewarmed medium containing desired doses of NPs for different time points (20 or 40 h).

Although a direct dose comparison between *in vivo* and *in vitro* studies is challenging, we chose CeO_2 NP doses that represent the lower end of what is reported in the literature.[16,19,39,40] Furthermore, the doses used for our assays (0.5–10 μg/mL, *i.e.*, 2.9–58 μM) lie in the possible long-term human exposure range, because CeO_2 is cleared from human lungs over a period of many years.[41]

In experiments requiring pretreatment with inhibitors, cells were first incubated with inhibitor containing *ex vivo* medium as described below and then exposed to fresh NP suspensions in medium containing inhibitors. At the end of the treatment period cells were trypsinated using 0.025% trypsin-EDTA (Invitrogen). The action of trypsin was inhibited using 10% fetal bovine serum (Sigma Aldrich, St. Louis, MO, USA). In some experiments, polyethylene glycol-coated catalase (PEG-catalase, Sigma Aldrich, St. Louis, MO, USA) pretreatment was done for 30 min (1000 IU), and then cells were treated with CeO_2 NPs. A similar protocol with a 2 h preincubation was followed for p53 inhibitor (pifithrin-alpha) and autophagy inhibitor wortmannin (both from Sigma Aldrich).

TEM Analysis of NP–Cell Interaction. Human peripheral blood monocytes were grown in two chamber cell culture slides and treated with different concentrations of CeO_2 NPs for 40 h. The cells were fixed in 3% gluteraldehyde. Thin sections (60–90 nm) were cut and placed on Formvar copper grids and then stained with uranyl acetate and lead citrate. After staining, the sections were examined on a FEI Tecnai 110 kV microscope at 80 kV, and digital photomicrographs were taken.

Cell Viability Analysis. Cells were seeded in 96-well plates (at 50 000 cells/well density) and treated with different concentrations (0.5–10 μg/mL) of CeO_2 NPs for 20 or 40 h. Cells were then incubated with 10 μM calcein-AM (Invitrogen) for 1 h. The green fluorescence from viable cells (produced due to esterase activity in the living cells) was analyzed at 485 nm excitation and 530 nm emission wavelengths. NP-treated cells without calcein-AM and calcein-AM alone with NPs (without cells) were also analyzed to rule out possible interferences with the assay. The results are presented as percent of control.

DNA Fragmentation (Sub-G1 Peak) Analysis. Sub-G1 peak analysis was performed according to the method described previously.[42] Cells were analyzed using a BD Facsort flow cytometer for 535 nm excitation and 617 nm emission wavelengths for propidium iodide (PI). At least 7500 cells were analyzed to determine the percentage of cells in the sub-G1 region.

Annexin-V/PI Staining. Annexin-V/PI labeling was performed according to the manufacturer's recommendations (Invitrogen). Analysis was performed on a BD FACSAria II instrument. At least 10 000 cells were analyzed to determine the percentage of apoptotic cells. The results are presented as percentage of apoptotic cells (early + late apoptotic cells). However, it is noteworthy that the majority of the positive cells (>90%) were early apoptotic cells.

Mitochondrial Membrane Potential ($\Delta\Psi_m$) Changes. Changes in $\Delta\Psi_m$ were monitored after staining with a JC-1 probe (Invitrogen) as described elsewhere.[43] Analysis was performed on a BD FACSAria II instrument.

Immunocytochemistry. Staining for activated Bax and microtubule-associated protein 1 light chain 3 (LC3B) was performed on paraformaldehyde (4%)-fixed cells as described previously.[44] Mouse anti-Bax (6A7, Sigma Aldrich) and rabbit recombinant oligoclonal antibody (Invitrogen) were used as primary antibodies, and Alexa Fluor 488 IgG (Invitrogen) was used as secondary antibodies. Nuclei were stained with Hoechst 33258 (1 μg/mL). Autophagic vesicle formation was also confirmed after labeling

with Enzo Autophagy kit reagents (MDC and Hoechst). Live cells were loaded with MitoTracker Red (Invitrogen) and fixed for co-localization analysis with activated Bax. Images were captured using a Zeiss−Axiovert40 CFL microscope and processed using Image J software (NIH, USA).

Flow Cytometery for Apoptosis Inducing Factor. AIF antibody analysis was performed on flow cytometery using anti-AIF FITC antibody and isotype control antibody from Santa Cruz Biotechnology (Santa Cruz, CA, USA). Analysis was performed on a BD FACSAria II at 488 nm excitation and 530 nm emission wavelengths. Results are presented as fold increase in mean fluorescence intensity values with respect to control.

LysoTracker Red Uptake Assay. Autophagy was assessed through monitoring LysoTracker Red (Invitrogen) uptake (normalized to CellTracker Green) in CeO_2 NP-treated cells using a previously described method.[45] The cells were analyzed at 530/590 nm excitation/emission for LysoTracker Red and 485/520 nm for CellTracker Green using a Biotech Powerwave XS plate reader.

Statistical Analysis. Every experiment was repeated using cells from 3 to 5 human subjects. Data are presented as average ± SD. Each experimental condition was done in triplicate for each individual. Data are analyzed by analysis of variance (ANOVA) followed by the Bonferroni test for multiple comparisons using Graphpad software (Graphpad Prism 4.01, Graphpad Software Inc., San Diego, CA, USA). A level of $p < 0.05$ (two-tailed) was considered significant.

Conflict of Interest: The authors declare no competing financial interest.

Acknowledgment. This work was supported (in part) by the Intramural Research Program of the NIH, National Institute of Environmental Health Sciences (NIEHS). We wish to gratefully acknowledge all volunteers who participated in the study. We also thank Nicole Edwards and Gina Musselwhite for support in patient recruitment, Carl Bortner, Maria Sifre, Kevin Katen, Connie Cummings, and Deloris Sutton for technical assistance. Sue Edelstein is acknowledged for help with artwork.

Supporting Information Available: Supplementary experimental details. This material is available free of charge *via* the Internet at http://pubs.acs.org.

REFERENCES AND NOTES

1. Yu, J. C.; Zhang, L.; Lin, J. Direct Sonochemical Preparation of High-Surface-Area Nanoporous Ceria and Ceria-Zirconia Solid Solutions. *J. Colloid Interface Sci.* **2003**, *260*, 240–243.
2. Khan, S. B.; Faisal, M.; Rahman, M. M.; Jamal, A. Exploration of CeO Nanoparticles as a Chemi-Sensor and Photo-Catalyst for Environmental Applications. *Sci. Total Environ.* **2011**, *409*, 2987–2992.
3. Izu, N.; Shin, W.; Matsubara, I.; Murayama, N. Development of Resistive Oxygen Sensors Based on Cerium Oxide Thick Film. *J. Electroceram.* **2004**, *13*, 703–706.
4. Corma, A.; Atienzar, P.; Garcia, H.; Chane-Ching, J. Y. Hierarchically Mesostructured Doped CeO_2 with Potential for Solar-Cell Use. *Nat. Mater.* **2004**, *3*, 394–397.
5. Kosynkin, V. D.; Arzgatkina, A. A.; Ivanov, E. N.; Chtoutsa, M. G.; Grabko, A. I.; Kardapolov, A. V.; Sysina, N. A. The Study of Process Production of Polishing Powder Based on Cerium Dioxide. *J. Alloys Compd.* **2000**, *303*, 421–425.
6. Korsvik, C.; Patil, S.; Seal, S.; Self, W. T. Superoxide Dismutase Mimetic Properties Exhibited by Vacancy Engineered Ceria Nanoparticles. *Chem. Commun. (Cambridge, UK)* **2007**, 1056–1058.
7. Das, M.; Patil, S.; Bhargava, N.; Kang, J. F.; Riedel, L. M.; Seal, S.; Hickman, J. J. Auto-Catalytic Ceria Nanoparticles Offer Neuroprotection to Adult Rat Spinal Cord Neurons. *Biomaterials* **2007**, *28*, 1918–1925.
8. Tarnuzzer, R. W.; Colon, J.; Patil, S.; Seal, S. Vacancy Engineered Ceria Nanostructures for Protection from Radiation-Induced Cellular Damage. *Nano Lett.* **2005**, *5*, 2573–2577.
9. Chen, J.; Patil, S.; Seal, S.; McGinnis, J. F. Rare Earth Nanoparticles Prevent Retinal Degeneration Induced by Intracellular Peroxides. *Nat. Nanotechnol.* **2006**, *1*, 142–150.
10. Rzigalinski, B. A.; Meehan, K.; Davis, R. M.; Xu, Y.; Miles, W. C.; Cohen, C. A. Radical Nanomedicine. *Nanomedicine (London)* **2006**, *1*, 399–412.
11. Park, B.; Donaldson, K.; Duffin, R.; Tran, L.; Kelly, F.; Mudway, I.; Morin, J. P.; Guest, R.; Jenkinson, P.; Samaras, Z.; *et al.* Hazard and Risk Assessment of a Nanoparticulate Cerium Oxide-Based Diesel Fuel Additive−a Case Study. *Inhal. Toxicol.* **2008**, *20*, 547–566.
12. Health Effects Institute (HEI). *Evaluation of Human Health Risk from Cerium Added to Diesel Fuel*; Communication 9, **2001**.
13. Cassee, F. R.; van Balen, E. C.; Singh, C.; Green, D.; Muijser, H.; Weinstein, J.; Dreher, K. Exposure, Health and Ecological Effects Review of Engineered Nanoscale Cerium and Cerium Oxide Associated with Its Use as a Fuel Additive. *Crit. Rev. Toxicol.* **2011**, *41*, 213–229.
14. Organisation for Economic Co-operation and Development (OECD). *List of Manufactured Nanomaterials and List of End Points for Phase One of the OECD Testing Programme*; **2008**.
15. Ma, J. Y.; Zhao, H.; Mercer, R. R.; Barger, M.; Rao, M.; Meighan, T.; Schwegler-Berry, D.; Castranova, V.; Ma, J. K. Cerium Oxide Nanoparticle-Induced Pulmonary Inflammation and Alveolar Macrophage Functional Change in Rats. *Nanotoxicology* **2011**, *5*, 312–325.
16. Park, E. J.; Choi, J.; Park, Y. K.; Park, K. Oxidative Stress Induced by Cerium Oxide Nanoparticles in Cultured Beas-2b Cells. *Toxicology* **2008**, *245*, 90–100.
17. Cho, W. S.; Duffin, R.; Poland, C. A.; Howie, S. E.; MacNee, W.; Bradley, M.; Megson, I. L.; Donaldson, K. Metal Oxide Nanoparticles Induce Unique Inflammatory Footprints in the Lung: Important Implications for Nanoparticle Testing. *Environ. Health Perspect.* **2010**, *118*, 1699–1706.
18. Hirst, S. M.; Karakoti, A. S.; Tyler, R. D.; Sriranganathan, N.; Seal, S.; Reilly, C. M. Anti-Inflammatory Properties of Cerium Oxide Nanoparticles. *Small* **2009**, *5*, 2848–2856.
19. Xia, T.; Kovochich, M.; Liong, M.; Madler, L.; Gilbert, B.; Shi, H.; Yeh, J. I.; Zink, J. I.; Nel, A. E. Comparison of the Mechanism of Toxicity of Zinc Oxide and Cerium Oxide Nanoparticles Based on Dissolution and Oxidative Stress Properties. *ACS Nano* **2008**, *2*, 2121–2134.
20. Lowe, S. W.; Lin, A. W. Apoptosis in Cancer. *Carcinogenesis* **2000**, *21*, 485–495.
21. Mattson, M. P. Apoptosis in Neurodegenerative Disorders. *Nat. Rev. Mol. Cell Biol.* **2000**, *1*, 120–129.
22. Adrie, C.; Bachelet, M.; Vayssier-Taussat, M.; Russo-Marie, F.; Bouchaert, I.; Adib-Conquy, M.; Cavaillon, J. M.; Pinsky, M. R.; Dhainaut, J. F.; Polla, B. S. Mitochondrial Membrane Potential and Apoptosis Peripheral Blood Monocytes in Severe Human Sepsis. *Am. J. Respir. Crit. Care Med.* **2001**, *164*, 389–395.
23. Li, C.; Liu, H.; Sun, Y.; Wang, H.; Guo, F.; Rao, S.; Deng, J.; Zhang, Y.; Miao, Y.; Guo, C.; *et al.* Pamam Nanoparticles Promote Acute Lung Injury by Inducing Autophagic Cell Death through the Akt-Tsc2-Mtor Signaling Pathway. *J. Mol. Cell Biol.* **2009**, *1*, 37–45.
24. Zhang, Q.; Yang, W.; Man, N.; Zheng, F.; Shen, Y.; Sun, K.; Li, Y.; Wen, L. P. Autophagy-Mediated Chemosensitization in Cancer Cells by Fullerene C60 Nanocrystal. *Autophagy* **2009**, *5*, 1107–1117.
25. Stern, S. T.; Zolnik, B. S.; McLeland, C. B.; Clogston, J.; Zheng, J.; McNeil, S. E. Induction of Autophagy in Porcine Kidney Cells by Quantum Dots: A Common Cellular Response to Nanomaterials? *Toxicol. Sci.* **2008**, *106*, 140–152.
26. Man, N.; Yu, L.; Yu, S. H.; Wen, L. P. Rare Earth Oxide Nanocrystals as a New Class of Autophagy Inducers. *Autophagy* **2010**, *6*, 310–311.
27. Maiuri, M. C.; Galluzzi, L.; Morselli, E.; Kepp, O.; Malik, S. A.; Kroemer, G. Autophagy Regulation by P53. *Curr. Opin. Cell Biol.* **2010**, *22*, 181–185.
28. Tasdemir, E.; Chiara Maiuri, M.; Morselli, E.; Criollo, A.; D'Amelio, M.; Djavaheri-Mergny, M.; Cecconi, F.; Tavernarakis, N.; Kroemer, G. A Dual Role of P53 in the Control of Autophagy. *Autophagy* **2008**, *4*, 810–814.

29. Sanfins, E.; Dairou, J.; Hussain, S.; Busi, F.; Chaffotte, A. F.; Rodrigues-Lima, F.; Dupret, J. M. Carbon Black Nanoparticles Impair Acetylation of Aromatic Amine Carcinogens through Inactivation of Arylamine N-Acetyltransferase Enzymes. *ACS Nano* **2011**, *5*, 4504–4511.
30. Zhang, B.; Xing, Y.; Li, Z.; Zhou, H.; Mu, Q.; Yan, B. Functionalized Carbon Nanotubes Specifically Bind to Alpha-Chymotrypsin's Catalytic Site and Regulate Its Enzymatic Function. *Nano Lett.* **2009**, *9*, 2280–2284.
31. Gozuacik, D.; Kimchi, A. Autophagy as a Cell Death and Tumor Suppressor Mechanism. *Oncogene* **2004**, *23*, 2891–2906.
32. Gomes, L. C.; Scorrano, L. Mitochondrial Elongation during Autophagy: A Stereotypical Response to Survive in Difficult Times. *Autophagy* **2011**, *7*, 1251–1253.
33. Green, D. R.; Reed, J. C. Mitochondria and Apoptosis. *Science* **1998**, *281*, 1309–1312.
34. Cande, C.; Cecconi, F.; Dessen, P.; Kroemer, G. Apoptosis-Inducing Factor (AIF): Key to the Conserved Caspase-Independent Pathways of Cell Death? *J. Cell Sci.* **2002**, *115*, 4727–4734.
35. Samuelsen, M.; Cecilie Nygaard, U.; Lovik, M. Particles from Wood Smoke and Road Traffic Differently Affect the Innate Immune System of the Lung. *Inhal. Toxicol.* **2009**, *21*, 943–951.
36. Lucarelli, M.; Gatti, A. M.; Savarino, G.; Quattroni, P.; Martinelli, L.; Monari, E.; Boraschi, D. Innate Defence Functions of Macrophages Can Be Biased by Nano-Sized Ceramic and Metallic Particles. *Eur. Cytokine Netw.* **2004**, *15*, 339–346.
37. Hollingsworth, J. W.; Maruoka, S.; Li, Z.; Potts, E. N.; Brass, D. M.; Garantziotis, S.; Fong, A.; Foster, W. M.; Schwartz, D. A. Ambient Ozone Primes Pulmonary Innate Immunity in Mice. *J. Immunol.* **2007**, *179*, 4367–4375.
38. Ireland, J. M.; Unanue, E. R. Autophagy in Antigen-Presenting Cells Results in Presentation of Citrullinated Peptides to Cd4 T Cells. *J. Exp. Med.* **2011**, *208*, 2625–2632.
39. Celardo, I.; De Nicola, M.; Mandoli, C.; Pedersen, J. Z.; Traversa, E.; Ghibelli, L. Ce(3)+ Ions Determine Redox-Dependent Anti-Apoptotic Effect of Cerium Oxide Nanoparticles. *ACS Nano* **2011**, *5*, 4537–4549.
40. Gojova, A.; Lee, J. T.; Jung, H. S.; Guo, B.; Barakat, A. I.; Kennedy, I. M. Effect of Cerium Oxide Nanoparticles on Inflammation in Vascular Endothelial Cells. *Inhal. Toxicol.* **2009**, *21*), 123–130.
41. Pairon, J. C.; Roos, F.; Iwatsubo, Y.; Janson, X.; Billon-Galland, M. A.; Bignon, J.; Brochard, P. Lung Retention of Cerium in Humans. *Occup. Environ. Med.* **1994**, *51*, 195–199.
42. Hussain, S.; Boland, S.; Baeza-Squiban, A.; Hamel, R.; Thomassen, L. C.; Martens, J. A.; Billon-Galland, M. A.; Fleury-Feith, J.; Moisan, F.; Pairon, J. C.; *et al*. Oxidative Stress and Proinflammatory Effects of Carbon Black and Titanium Dioxide Nanoparticles: Role of Particle Surface Area and Internalized Amount. *Toxicology* **2009**, *260*, 142–149.
43. Smiley, S. T.; Reers, M.; Mottola-Hartshorn, C.; Lin, M.; Chen, A.; Smith, T. W.; Steele, G. D., Jr.; Chen, L. B. Intracellular Heterogeneity in Mitochondrial Membrane Potentials Revealed by a J-Aggregate-Forming Lipophilic Cation Jc-1. *Proc. Natl. Acad. Sci. U. S. A.* **1991**, *88*, 3671–3675.
44. Hussain, S.; Thomassen, L. C.; Ferecatu, I.; Borot, M. C.; Andreau, K.; Martens, J. A.; Fleury, J.; Baeza-Squiban, A.; Marano, F.; Boland, S. Carbon Black and Titanium Dioxide Nanoparticles Elicit Distinct Apoptotic Pathways in Bronchial Epithelial Cells. *Part. Fibre Toxicol.* **2010**, *7*, 10.
45. Neun, B. W.; Stern, S. T. Monitoring Lysosomal Activity in Nanoparticle-Treated Cells. *Methods Mol. Biol.* **2011**, *697*, 207–212.